

Study of nuclei in the vicinity of the “Island of Inversion” through fusion-evaporation reaction

R. Chakrabarti,¹ S. Mukhopadhyay,^{1,*} Krishichayan,^{1,†} A. Chakraborty,^{1,‡}
A. Ghosh,¹ S. Ray,¹ S.S. Ghugre,¹ A.K. Sinha,¹ L. Chaturvedi,²
A.Y. Deo,³ I. Mazumdar,³ P.K. Joshi,³ R. Palit,³ Z. Naik,³ S. Kumar,⁴
N. Madhavan,⁵ R.P. Singh,⁵ S. Muralithar,⁵ B.K. Yogi,⁶ and U. Garg⁷

¹*UGC-DAE Consortium for Scientific Research,
Kolkata Centre, Kolkata 700098, INDIA*

²*Department of Physics, Pt. Ravishankar University, Raipur 492010, INDIA*

³*Tata Institute of Fundamental Research, Mumbai 400005, INDIA*

⁴*Department of Physics and Astrophysics,
University of Delhi, Delhi 110007, INDIA*

⁵*Inter University Accelerator Centre,
Aruna Asaf Ali Marg, New Delhi 110067, INDIA*

⁶*Department of Physics, Govt. College, Kota 324009, INDIA*

⁷*Department of Physics, University of Notre Dame, Notre Dame, IN 46556, USA*

(Dated: June 2, 2018)

Abstract

We report the first observation of high-spin states in nuclei in the vicinity of the “island of inversion”, populated via the $^{18}\text{O}+^{18}\text{O}$ fusion reaction at an incident beam energy of 34 MeV. The fusion reaction mechanism circumvents the limitations of non-equilibrated reactions used to populate these nuclei. Detailed spin-parity measurements in these difficult to populate nuclei have been possible from the observed coincidence anisotropy and the linear polarization measurements. The spectroscopy of $^{33,34}\text{P}$ and ^{33}S is presented in detail along with the results of calculations within the shell model framework.

PACS numbers: 21.20.Lv, 23.20.En, 23.20.Gq, 21.60.Cs, 27.30.+t

*Current affiliation: Department of Physics, Mississippi State University, Mississippi State, MS 39762, USA.

†Current affiliation: Cyclotron Institute, Texas A&M University, College Station, Texas 77843, USA

‡Current affiliation: Department of Physics, Krishnath College, Behrampore 742101, INDIA.

I. INTRODUCTION

Neutron-rich nuclei are currently of great interest as they exhibit structural properties very different from nuclei near the β -stability line. Evolving shell gaps and disappearance of magic numbers seen in neutron-rich nuclei challenge the conventional shell model theory. The “island of inversion” comprised of neutron-rich isotopes of Mg, Na, and Ne with $N \sim 20$ is one of the best examples of such unexpected structure changes observed in nuclei with large neutron-proton asymmetry. Investigations into the extent of this island and the transition region around it will lead to a greater understanding of the evolution of the structure of the atomic nucleus.

Nuclei in and around the “island of inversion” have in general been studied using transfer/deep inelastic reaction [1–5], or β -decay [6] or heavy ion inelastic scattering or deuteron inelastic scattering [7]. However such non-equilibrated reactions have certain limitations, like contamination from dominant fusion-evaporation channels, low production cross-sections, low spin population and coincident emissions from the binary partner. The above limitations can be circumvented to a very large degree by using fusion-evaporation reactions with a neutron-rich target and a neutron-rich projectile. In this paper we present the results of a spectroscopic investigation of nuclei in the vicinity of the “island of inversion” ($^{33,34}\text{P}$ and ^{33}S), populated via the fusion-evaporation reaction.

II. EXPERIMENTAL METHOD

$^{33,34}\text{P}$ and ^{33}S nuclei were populated utilizing the $^{18}\text{O}+^{18}\text{O}$ reaction. The ^{18}O beam at an incident energy of 34 MeV was provided by the 14 UD BARC-TIFR Pelletron facility at TIFR, Mumbai. The choice of the incident energy was determined by the earlier reported excitation function measurements [8] which indicate a considerable cross-section for these nuclei at this incident energy. The neutron-rich ^{18}O target was prepared by heating a 50 mg/cm²-thick Ta foil in an atmosphere of enriched Oxygen to form Ta₂O₅. The total ^{18}O equivalent thickness was estimated to be 1.6 mg/cm² on both sides of the Ta foil. The de-exciting γ rays were detected by an array of 7 Compton-suppressed Clover detectors placed at $\sim 30^\circ$, $\sim 60^\circ$, $\sim 90^\circ$, $\sim 120^\circ$ and $\sim 150^\circ$ with respect to the beam direction in the median plane. An event was recorded when at least 2 Clovers fired in coincidence. A total of ~ 1 bil-

lion such γ - γ coincidences were recorded. The data were recorded using CAMAC based data acquisition system LAMPS [9] and analyzed using IUCSORT [10–12] and RADWARE [13] software packages. The data were pre-sorted to correct for any on-line drifts to ensure that there were relatively no gain changes between any two list mode data sets within the experiment and, then, were precisely gain matched to ensure that data from each detector had a constant energy dispersion. The energy calibration was performed using radioactive sources ^{152}Eu and ^{133}Ba and beam-off radioactivity data. The data were sorted into symmetric and asymmetric γ - γ matrices. The genetic correlation between the de-exciting γ rays was established from the symmetric γ - γ matrix after background subtraction and efficiency correction. The asymmetric matrices were used to assign the spin and parity for the observed levels on the basis of angular correlation and the linear polarization measurements, as described in the next section.

III. EXPERIMENTAL RESULTS

A. Determination of spins and parities

The multipolarity assignments have been performed from the observed coincidence angular correlations. Assuming pure (stretched) transition, the coincidence intensity anisotropy can be used to distinguish between $\Delta J = 1$ and $\Delta J = 2$ transitions. A qualitative assignment for the multipolarity of the γ -transition from the angular correlation measurements is obtained following the procedure detailed in Ref. [14]. The experimental R_{DCO} in the present work is defined as:

$$R_{DCO} = \frac{I_{\gamma_1}(\text{at } \theta \text{ gated by } \gamma_2 \text{ at } 90^\circ)}{I_{\gamma_1}(\text{at } 90^\circ \text{ gated by } \gamma_2 \text{ at } \theta)} \quad (1)$$

where θ is 30° and 150° . When the gating transition (γ_2) is a stretched quadrupole transition, $R_{DCO} \sim 1$ for a pure quadrupole (γ_1) and ~ 0.5 for stretched pure dipole transition (γ_1). Similarly, a gate on a dipole transition would result in $R_{DCO} \sim 2$ for a pure quadrupole and ~ 1 for a pure dipole transition. These intensity ratios were obtained from the angle-dependent γ - γ matrices assuming stretched transition for the gates and after incorporating necessary efficiency corrections. The experimental R_{DCO} values determined from quadrupole and dipole gates have been plotted for several transitions belonging to $^{33,34}\text{P}$, $^{33,34}\text{S}$ in Fig. 1

and Fig. 2 respectively. The present statistics did not permit us to extend these measurements to the weak transitions. As seen from the figures, it is possible to distinguish between $\Delta J = 1$, and $\Delta J = 2$ transition following the above procedure. For mixed transitions the plot essentially provides a qualitative way of determining the dominant multipolarity considering the proximity of the R_{DCO} value to the $\Delta J = 1$ or the $\Delta J = 2$ line.

The angular correlation measurement is not sensitive to the electric or magnetic character of the radiation. The information on this was obtained from the linear polarization measurements. Clover detectors have an advantage over conventional single crystal detectors as they allow such measurements to be made.

The angular distribution of linearly polarized gamma rays from an axially oriented ensemble of nuclei is given by [15, 16]

$$W(\theta, \psi) = \frac{d\Omega}{8\pi} \sum_{\lambda=even} B_{\lambda} U_{\lambda} \left[A_{\lambda} P_{\lambda}(\cos\theta) + 2A_{\lambda 2} P_{\lambda 2}^{(2)}(\cos\theta) \cos 2\psi \right] \quad (2)$$

where B_{λ} are orientation tensors describing the degree of orientation of the parent nucleus and U_{λ} are deorientation coefficients. P_{λ} are the ordinary Legendre polynomials and $P_{\lambda 2}^{(2)}$ are the unnormalized associated Legendre polynomials. A_{λ} are angular distribution coefficients which depend on the spin of the initial and final state and the multipolarity of the γ -transition. The coefficients $A_{\lambda 2}$ depend on the electromagnetic character of the radiation [17]. θ is the angle that the electric vector of the emitted quanta makes with the orientation axis and ψ is the angle between the electric vector E of the emitted quanta and the reaction plane (Fig. 3).

The degree of linear polarization $P\theta$ of a γ ray is defined as the difference between the intensities of the radiation presenting an electric vector parallel to the reaction plane ($\psi = 0^{\circ}$) and that with an electric vector perpendicular to the plane ($\psi = 90^{\circ}$) [17–19]:

$$P(\theta) = \frac{W(\theta, \psi = 0) - W(\theta, \psi = \pi/2)}{W(\theta, \psi = 0) + W(\theta, \psi = \pi/2)} \quad (3)$$

where the normalization is such that $-1 \leq P(\theta) \leq +1$.

$P(\theta) = 0$ for an unpolarized γ -ray and has a maximum value at $\theta = 90^{\circ}$,

$$P_{cal}(90^{\circ}) = \pm \frac{3a_2 H_2 - 7.5a_4 H_4}{2 - a_2 + 0.75a_4} \quad (4)$$

where a_2 and a_4 are the angular distribution coefficients and the H_2 and H_4 coefficients depend on the initial and final spin and the mixing ratio, δ [20, 21].

Experimentally linear polarization of gamma rays was detected and measured through Compton scattering [17]. The differential Compton scattering cross-section is given by [17]

$$\frac{d\sigma}{d\Omega}(\nu, \chi) = \frac{r_0^2}{2} \left(\frac{E}{E_0} \right)^2 \left[\frac{E_0}{E} + \frac{E}{E_0} - 2 \sin^2 \nu \cos^2 \chi \right] \quad (5)$$

where r_0 is the classical electron radius, ν is the Compton scattering angle with respect to the direction of the incident γ ray, and χ is the angle between the electric vector E of the primary radiation and the scattering plane defined by the direction of the incident and the scattered photons (Fig. 3). This cross-section is relatively high and polarization sensitive for a wide photon energy range. Maximum scattering occurs at $\chi = 90^\circ$.

The Clover detectors used in the experiment acted effectively as Compton polarimeters. The detectors placed at $\sim 90^\circ$ were particularly useful since polarization is maximum in that direction. Each crystal of a Clover detector acts as a scatterer and the two adjacent crystals act as the absorbers. The asymmetry between the perpendicular and parallel scattering with respect to the reaction plane distinguishes between electric and magnetic transitions. The experimental asymmetry or Δ_{IPDCO} (IPDCO stands for ‘‘Integrated Polarizational-Directional Correlation from oriented nuclei’’) at 90° between perpendicular and parallel coincidence rates is defined [19] as

$$\Delta_{IPDCO} = \frac{aN_\perp - N_\parallel}{aN_\perp + N_\parallel} \quad (6)$$

where N_\perp and N_\parallel are the number of photons with a given energy scattered along the direction perpendicular and parallel to the reaction plane, respectively, in the detectors placed at $\sim 90^\circ$ and in coincidence with another photon detected in at least one other detector in the array. This is called an integrated PDCO because the polarization of one γ quantum is measured and the information is integrated over all the possible emission directions of the accompanying coincident radiation.

‘‘ a ’’ denotes the correction due to the asymmetry in response of the clover segments. This factor is energy dependent ($a = a_0 + a_1 E_\gamma$), and is determined using a radioactive source (having no spin alignment) under similar conditions. This correction is defined as [18, 19]

$$a = \frac{N_\parallel(\text{unpolarized})}{N_\perp(\text{unpolarized})} \quad (7)$$

The values for a_0 and a_1 for the present experimental setup were 1.00007(0.00698) and $7.89667 \times 10^{-7} \text{ keV}^{-1}$ (5.61462×10^{-7}) respectively.

Δ_{IPDCO} values were evaluated from asymmetric γ - γ matrices whose one axis corresponds to the perpendicular or parallel scattered events in the clovers at $\sim 90^\circ$ and the other axis corresponds to the total energy recorded in any of the other detectors. Gates were put on the full energy peaks of the perpendicular and parallel matrices to obtain spectra representing either perpendicular or parallel scattering respectively, and from these, the N_\perp and N_\parallel values were obtained for each transition. Fig. 4 is a representative background subtracted difference spectrum of perpendicular and parallel gates. The positive peaks indicate electric transitions whereas negative peaks indicate magnetic transitions.

The linear polarization is related to the asymmetry by the polarization sensitivity $Q(E_\gamma)$ as [18, 19]

$$\Delta_{IPDCO} = PQ(E_\gamma) \quad (8)$$

$Q(E_\gamma)$ is dependent on the incident gamma-ray energy and the geometry of the polarimeter and its values, were obtained for a similar setup as reported by Palit *et al.* [22]. The theoretical polarizations were determined using eq.(4) by calculating the angular distribution coefficients a_2 , a_4 and the H_2 , H_4 functions for each value of the multipole mixing ratio δ using the formalism given in Refs. [20, 21, 23]. The theoretical Δ_{IPDCO} values were obtained from the theoretical polarization values using eq.(8), and are plotted along with the experimentally obtained Δ_{IPDCO} values as a function of E_γ in Fig. 5 for several strong transitions in ^{34}S , ^{33}P and ^{33}S . The results show a good agreement between the theoretical and experimental values. At a given energy, a positive value of the asymmetry parameter indicates an electric transition, a negative value indicates a magnetic transition and a near-zero value is indicative of an admixture.

The calculation of theoretical polarization requires two inputs, *viz.*, the width of the m -state distribution and the mixing ratios. Polarization depends significantly on the distribution of the nuclear state over its magnetic substates. When the alignment is partial, the angular distribution coefficients for complete alignment [23] have to be multiplied with the attenuation coefficients as formulated by Der Mateosian and Sunyar [21], which depend on the factor σ/J where σ is the width of the distribution of the m -states, assuming a Gaussian distribution [23]. The choice of σ/J was made following the simultaneous analysis of the R_{DCO} and Δ_{IPDCO} values for several transitions of known spin and parity. Fig. 6 and Fig. 7 depict the determination of σ/J for one such transition, the 1066-keV $[5^- \rightarrow 3^-, \delta = 0]$ belonging to ^{34}S . This nucleus has been populated with substantial cross-section in

the present experiment and its level scheme has been extensively reported earlier by Mason *et al.* [24]. The theoretical R_{DCO} values were obtained using the code ANGCOR [25] as a function of σ/J . Fig. 6 represents the comparison of the theoretical R_{DCO} values with the experimentally obtained values. As seen from the figure, a value of $\sigma/J \sim 0.35 - 0.45$ appears to be reasonable. A similar plot has been made for the Δ_{IPDCO} values of the same transition in Fig. 7. Here also the theoretical values agree with the experimental ones in the same range. This exercise was repeated for other transitions in ^{34}S of known mixing ratios [26]. It was observed that a value of $\sigma/J = 0.4$ consistently reproduced the observed R_{DCO} and Δ_{IPDCO} values and hence this value was used in all our calculations.

Fig. 8 shows the theoretical asymmetry values for a pure E2 transition ($J^\pi = 2^+ \rightarrow 0^+$) as a function of mixing ratio at different values of σ/J . The shaded area gives the range of observed Δ_{IPDCO} values for the known 2127-keV, E2 transition ($2^+ \rightarrow 0^+$) in ^{34}S . An increase in σ/J decreases polarization. At $\sigma/J = 0.6$ the theoretical values are not consistent with the experimental values. The theoretical asymmetry value at $\delta = 0$ for $\sigma/J = 0.4$ lies well within the experimentally observed range. This also justifies our choice of σ/J .

The calculated and observed R_{DCO} and Δ_{IPDCO} values for several strong transitions in ^{34}S , ^{33}P and ^{33}S are given in Table I. The R_{DCO} and Δ_{IPDCO} values are consistently reproduced within error bars in each case.

Wherever quantitative measurements were not possible due to insufficient statistics, parity assignment was done qualitatively from the corresponding gated perpendicular and parallel spectra. When gates were put on coincident gamma transitions and more counts were observed in the perpendicular gated spectra than in the parallel, the observed γ -ray was assigned an electric nature. The reverse was true for assignment of a magnetic nature. Thus the previously reported spin-parities of the levels in $^{33,34}\text{S}$ and $^{33,34}\text{P}$ that were observed in the present experiment, have been confirmed either quantitatively or qualitatively.

B. Level schemes

The nuclei populated in the experiment as determined from the projection spectra and supported by the beam-off radioactivity data were ^{34}S , ^{33}S , ^{34}P , ^{33}P , ^{32}P and ^{30}Si . Fig. 9 depicts the projection spectrum of the symmetric γ - γ matrix. The use of fusion evaporation reaction to populate the above-mentioned nuclei has clearly enhanced their production

compared to deep-inelastic/transfer reactions [5] as is evident from Fig. 10. The comparison also shows a much cleaner and contamination free spectrum obtained in the present experiment. Moreover, higher spin states have become accessible as a result of utilizing fusion evaporation reaction mechanism.

The level schemes of these nuclei have been extended with the addition of several new transitions. Figs. 11, 12 and 13 are spectra obtained by gating on the symmetric γ - γ matrix by the 429-keV, 186-keV, and 968-keV γ -rays belonging to ^{34}P , ^{33}P , and ^{33}S , respectively. The deduced level schemes are shown in Figs. 14, 15 and 16. The energies, relative intensities and assigned multiplicities of the observed transitions, the assigned excitation energies and spin-parities of the levels, and the γ -ray branching ratios for decay of those levels are listed in Table II.

A quantitative measure of R_{DCO} and/or linear polarization has not been possible for some transitions. In those cases, a qualitative assignment has been made as explained in the previous section. The multiplicities listed in TABLE II for such transitions are essentially the dominant multiplicity; the extent of mixing could not be determined. The present setup did not permit us to obtain the mixing ratios experimentally. However mixing ratio range has been deduced from the R_{DCO} and Δ_{IPDCO} values for some transitions in ^{34}P , as explained later. The comparison between theoretical and experimental R_{DCO} and Δ_{IPDCO} values in ^{34}S , ^{33}P , and ^{33}S is based on previously-reported mixing ratios (TABLE I).

1. ^{34}P

Previous investigations of the level structure of ^{34}P employed non-equilibrated reactions to populate this difficult to access $N = 19$ nucleus. These studies reported different subsets of the excited levels in ^{34}P . Ajzenberg-Selove *et al.* [27] were the first to report the excited states of ^{34}P at 423, 1605, 2225, 2309 and (3345) keV (± 10 keV) using the $^{34}\text{S}(t, ^3\text{He})^{34}\text{P}$ reaction. On the other hand, 429-, 1608- and 1178-keV gamma rays were identified by both Nathan *et al.* [6] and Pritychenko *et al.* [28] in β -decay and intermediate-energy Coulomb excitation measurements respectively. Pritychenko *et al.* [28] also observed a new 627-keV transition de-exciting the (2^+) level at 2225 keV. However the 1608-keV and 627-keV transition were not observed in any of the subsequent investigations using transfer and deep-inelastic reactions [1, 3, 5]. All the excited states of ^{34}P reported by Ollier *et al.* [3], except

the level at 4723 keV were observed in the present work. Several other strong transitions, of 679, 1444, 1607, 1638, 1646, 2325 and 3932 keV belonging to ^{34}P have been identified and placed in the level scheme by coincidence and intensity arguments. The placements of the new transitions were also facilitated to a large extent by the observation of cross-over transitions. The 1607-keV transition was found to be in coincidence with the 429- and 1876-keV transitions and hence is different from the 1608-keV transition reported by Nathan *et al.* [6] and Pritychenko *et al.* [28]. The 1046-keV transition reported by Ollier *et al.* [3] but not observed by Krishichayan *et al.* [5] has been observed in the present experiment, but with an energy of 1048-keV. Further, this transition exhibited a shape asymmetry at forward and backward angles, which is indicative of a lifetime of the order of a few pico-second for the 3353 keV level.

One of the main motivations of the present experiment was to undertake polarization and coincidence angular correlation measurements following fusion reaction to confirm the spin-parity assignment of the 2305-keV level in ^{34}P . In Ref. [5], we had assigned $J^\pi = 4^+$ to this level, whereas it had been assigned 4^- by earlier workers [2, 27]. The 429-keV was established as a magnetic dipole transition from the DCO and polarization analysis method described in the previous section. The 1876-keV γ ray de-exciting the 2305-keV level has a R_{DCO} value 1.62(26) (Fig. 2) and linear polarization measurements yielded a near-zero value for Δ_{IPDCO} , establishing it as a highly mixed ($L = 2, L' = 3$) transition for the first time (Fig. 19). This is also evident from the difference between the 429-keV gated perpendicular and parallel scattering spectra (Fig. 17), where the number of counts under 1876 keV peak is nearly zero. In such cases, the polarization measurements cannot distinguish between M2/E3 and E2/M3 mixing. Fig. 18 depicts the theoretical asymmetry curves for $2^+ \rightarrow 1^+$ M1/E2 radiation as a function of mixing ratio, at different values of σ/J . The shaded area represents the experimental dispersion in Δ_{IPDCO} of the 429-keV γ ray. At $\sigma/J = 0.4$, the theoretical values are consistent with experimental Δ_{IPDCO} values over the range $-8^\circ \leq \arctan(\delta) \leq 0^\circ$ and $49^\circ \leq \arctan(\delta) \leq 54^\circ$. However, as seen from Fig. 18, the mixing ratio predicted by the shell model (as detailed in the subsequent section and indicated by the vertical dotted line) limits the value to the former range. We have similarly plotted the theoretical asymmetry values for a M2/E3 mixing $4^- \rightarrow 2^+$ as a function of mixing ratio, at different values of σ/J (Fig. 19). The shaded area on this graph represents experimental range of Δ_{IPDCO} for the 1876-keV transition. The theoretical values are consistent with

the experimental values over the range $-46^\circ \leq \arctan(\delta) \leq -15^\circ$ and $50^\circ \leq \arctan(\delta) \leq 76^\circ$ for $\sigma/J = 0.4$. The latter range of very large mixing ratios being physically unreasonable, has not been considered. When we repeated this exercise considering a E2/M3 mixing, we obtained almost the same ranges of mixing ratios. Thus an unambiguous identification of the 1876-keV transition as M2/E3 or E2/M3 is not possible following this procedure. The Δ_{IPDCO} value at $\sigma/J = 0.4$ corresponding to the mixing ratio predicted by the shell model calculations (Section IV) does not lie within the aforementioned ranges in both cases. This mismatch has been discussed in detail in the subsequent section.

Fig. 20 shows the variation of theoretical R_{DCO} for the 1876-keV γ -ray as a function of its mixing ratio when the gate is on the 429-keV, the ground state transition. The three plots correspond to the three values of δ_{429} [$-0.14 \leq -0.07 \leq 0.0$] that were determined earlier from Fig. 18. The theoretical R_{DCO} values were computed using ANGCOR [25]. The horizontal lines mark the experimental range of R_{DCO} values for the 1876-keV transition, while the vertical lines indicate the range of mixing ratios for this transition as obtained from Fig. 19. As is evident from the graph, the mixing ratio range obtained from the analysis of the linear polarization measurements is also consistent with the angular correlation measurements. Thus, both these measurements are indicative of $-1.03 \leq \delta_{1876} \leq -0.27$.

Asai *et al.* [2] have reported the lifetime of the level at $E_x = 2.305$ MeV as $0.3 \text{ ns} \leq t_{1/2} \leq 2.5 \text{ ns}$. Combining this lifetime measurement with the mixing ratio range, that we have obtained for 1876-keV, we have calculated the experimental reduced transition probabilities assuming both M2/E3 and E2/M3 mixing. The calculations are presented in TABLE III. As is evident from the table, the lifetime measurements lead to unacceptable M3 strengths [29]. This supports an M2/E3 assignment for the 1876-keV transition and $J^\pi = 4^{(-)}$ to the 2305 keV level. This needs to be confirmed with precise lifetime measurements, however.

The qualitative linear polarization measurements for the 1607-, 1646-, 679- and 2325-keV transitions indicate an electric nature for them. The spin-parity assignments for the levels de-exciting via these transitions are based on the assumption of $J^\pi = 4^{(-)}$ for the 2305-keV level.

2. ^{33}P

This work reports the first polarization measurement for ^{33}P populated in a heavy-ion fusion reaction. The earlier light-ion induced reaction investigations had established the level structure up to a spin of $J^\pi = 11/2^-$ and $E_x \sim 5.6$ MeV [30]. We have been able to extend the yrast sequence up to $J^\pi = 17/2^{(+)}$ and $E_x \sim 8$ MeV due to the observation of two new transitions of energy 1298 keV (E2) and 1028 keV (M1). The multipolarities of these two transitions were assigned as quadrupole and dipole, respectively, on the basis of the observed R_{DCO} values. The parity measurements have been shown as tentative since only qualitative measurements were possible. The 1028-keV transition was identified as a magnetic transition due to its preferential scattering in the parallel direction as observed in 1298-keV gated perpendicular and parallel spectra. On the other hand, the 1298-keV transition was assigned an electric nature due to its preferential scattering in perpendicular direction. A full Doppler shift has been observed in the 1298-keV transition and hence, the lifetime of the 6938 keV level is expected to be much less as compared to the stopping time (\sim pico-second). Apart from these, several other new transitions, with energies (in ascending order) of 237, 247, 980, 994, 1008, 1312, 1825 (D), 2142 (Q) and 3605 keV were observed and placed in the decay scheme. The present statistics did not permit us to observe the weak transition to the $E_x \sim 5221$ -keV from the level at 5454 keV. We have also observed 1170- and 880-keV transitions which could not be placed in the decay scheme. It is worth mentioning that the single- (1868 keV) and double-escape (1358 keV) peaks corresponding to the 2379-keV transition were observed and the intensity of this γ -ray reported in TABLE II was obtained from the sum of the counts under the full photopeak and the two escape peaks. This was done as our efficiency measurements (performed with a ^{152}Eu source) did not have data points in this energy region where escape contribution becomes significant.

3. ^{33}S

Prior to this experiment ^{33}S has been studied via light ion reactions [31]. In this experiment, the level scheme of ^{33}S was extended with the addition of 6 new transitions of energy 597, 597, 603, 845 (E1), 1015 (E1) and 1931 keV respectively. The presence of a 597-keV transition in the 597-keV gated spectrum is indicative of a doublet. As a result it

was not possible to determine their individual intensities and the spin parity of the excited states that de-excite via these two transitions. The qualitative polarization and angular correlation measurements for the 845-keV and the 1015-keV transitions indicate that these are dipoles and electric in nature. Such sequences of electric transitions have been reported in neighbouring nuclei like ^{32}P [26]. The 1931-keV transition exhibits the fully Doppler shifted peak indicating a short lifetime (\ll pico-second, the stopping time) for the level at ~ 4867 keV. The present polarization and angular correlation measurements confirmed the previously assigned spin-parity of the 1968- and 2936-keV levels. The reported mixing ratios are consistent with the results of the present measurement (TABLE I).

IV. THEORETICAL RESULTS

Shell model calculations using the code NuShell@MSU [32] were performed to interpret the observed level structures of $^{33,34}\text{P}$ and ^{33}S . The valence space consisted of the $1d_{5/2}$, $1d_{3/2}$, $2s_{1/2}$, $1f_{7/2}$, $1f_{5/2}$, $2p_{3/2}$ and $2p_{1/2}$ orbitals outside a ^{16}O core. The “*sdp_fmw*” interaction, taken from the Warburton, Becker, Millener, and Brown (WBMB) *sd-pf* shell Hamiltonian [33], was used.

In ^{34}P the positive-parity states 1^+ and 2^+ , which are expected to be dominated by the pure *sd* configurations, are well reproduced within the full *sd*-space shell model calculations ($0\hbar\omega$) (using the *sdp_fmw* interaction) and are consistent with the *sd* calculation of Brown [34]. The predicted binding energy of the ground state is -191.971 MeV, which matches very well with the experimental value -192.04 MeV [34]. The mixing ratio of the 429-keV transition predicted by shell model is -0.0024, which is also within the range determined from our polarization measurements.

Excitations of nucleons from *sd* shell into *fp* shell are essential to explain the negative-parity states (minimum 1 particle in the *fp* shell) as well as the high-spin, positive-parity states (minimum 2 particles in the *fp* shell). Due to computational limitations, unrestricted calculations were not possible and only one particle could be excited to the *pf* shell ($1\hbar\omega$).

It has been reported by several authors that there is an overestimation of the *sd-pf* gap in the corresponding interaction which required the lowering of the single-particle energies of the *f* and *p* orbitals [24, 35]. No such attempt was made in the present calculation.

Fig. 21 shows a the comparison between the calculated and the experimental levels in ^{34}P .

The 7^+ state predicted by the shell model is at a very high excitation energy (11366 keV) and hence has not been included in the figure. As seen from Fig. 21, the high-spin positive-parity states are much higher in excitation energy than the corresponding experimental levels. This is likely due to our inability to excite more than one particle into the fp shell. There is a reasonable agreement in excitation energy between the $J^\pi = 4^-, 5^-, 6^-$ levels predicted by shell model and the observed 2305-, 3353- and 4630- keV levels, respectively. Thus, the theory corroborates our spin-parity assignments at least for the negative-parity states. However, the above shell model calculations failed to predict the mixed nature of the 1876-keV transition established from our polarization measurements. The shell model predicts an almost pure M2 nature for this transition [$\delta = -0.034$]. The B(M2) and B(E3) values obtained from shell model are 0.1816 W.u. and 0.2167 W.u., respectively, and, as seen from Table II, the B(E3) values are heavily under predicted, clearly reflecting this mismatch. We have also performed similar shell model calculations for the neighbouring $N = 19$ isotones viz., ^{37}Ar and ^{35}S where similar M2/E3 mixed transitions are reported (1611 keV ($J^\pi = 7/2^- \rightarrow 3/2^-$ in ^{37}Ar) and 1911 keV ($J^\pi = 7/2^- \rightarrow 3/2^-$ in ^{35}S) [26]. The results are summarized in TABLE IV. In all cases, the calculations predict very little mixing, unlike the experimental observations. The E3 transition strengths are several orders of magnitude higher than the corresponding shell model predictions. Clearly, there is a need to perform these calculations with a better Hamiltonian encompassing a realistic cross-shell interaction, and/or with a more complete wave function incorporating configurations arising from multi-particle excitations into the fp orbitals.

The $0\hbar\omega$ calculations for ^{33}P and ^{33}S reproduces the low-spin positive-parity states. However, the $1\hbar\omega$ calculations fail to generate the first experimentally-observed negative-parity state, $7/2^-$, in both nuclei. The predicted energies of the high-spin, negative-parity states are higher than the experimental values by several MeV.

V. CONCLUSIONS

The level structure of the generally difficult to access nuclei $^{33,34}\text{P}$ and ^{33}S has been investigated using heavy-ion fusion reaction which has resulted in a substantial enhancement in their production cross-sections. The level schemes of these nuclei have been considerably extended. Spin-parity assignments have been made following a consistent analysis of both

the coincidence angular correlation and linear polarization data. The results indicate that the 1876-keV transition de-exciting the 2305-keV level in ^{34}P is a mixed transition and plausibly has a M2/E3 admixture; however precise lifetime measurements would be required to confirm this assignment unambiguously. The shell model calculations emphasize the need for detailed microscopic calculations to understand the observed level sequences and mixing ratios. The deformed shell model could provide an insight into the observed level structures due to the occupation of deformation-driving orbitals such as $f_{7/2}$.

VI. ACKNOWLEDGEMENTS

The authors would like to thank all the participants who have helped set up the Clover array at TIFR. The help and co-operation received from Mr Kaushik Basu of UGC-DAE CSR during the experiment is gratefully acknowledged. We would like to thank the BARC-TIFR Pelletron staff for their excellent support during the experiment. We are thankful to Mr. J. P. Greene, ANL, U.S.A, for the ^{18}O target. Thanks are also due to Dr. W. P. Tan and Dr. Larry Lamm, Univ. of Notre Dame, U.S.A, for providing us the enriched ^{18}O cathode. Special thanks to Prof. Alex Brown for the indepth discussions and his views and comments on Shell model calculations.

-
- [1] B. Fornal *et al.*, Phys. Rev. C **49**, 2413 (1994).
 - [2] M. Asai, T. Ishii, A. Makishima, M. Ogawa, and M. Matsuda, Proceedings of the Third International Conference on Fission and Properties of Neutron-Rich Nuclei, edited by J. H. Hamilton, A. V. Ramayya, H. K. Carter (World Scientific, Singapore, 2002) pp. 295-297.
 - [3] J. Ollier *et al.*, Phys. Rev. C **71**, 034316 (2005).
 - [4] R. Broda, J. Phys. G: Nucl. Part. Phys. **32**, R151 (2006).
 - [5] Krishichayan *et al.*, Eur. Phys. J. A **29**, 151 (2006).
 - [6] A. M. Nathan and D. E. Alburger, Phys. Rev. C **15**, 1448 (1977).
 - [7] I. Iwasa *et al.*, Phys. Rev. C **67**, 064315 (2003).
 - [8] Y. Eyal and I. Dastrovosky, Nucl. Phys. A **179**, 594 (1972).
 - [9] *LAMPS*, <http://www.tifr.res.in/~pell/lamps.html#>.

- [10] N. S. Pattabiraman, S. N. Chintalapudi, and S. S. Ghugre, Nucl. Instrum. Methods Phys. Res. A, **526**, 432 (2004).
- [11] N. S. Pattabiraman, S. N. Chintalapudi, and S. S. Ghugre, Nucl. Instrum. Methods Phys. Res. A, **526**, 439 (2004).
- [12] N. S. Pattabiraman, S. S. Ghugre, S. K. Basu, U. Garg, S. Ray, A. K. Sinha, and S. Zhu, Nucl. Instrum. Methods Phys. Res. A, **562**, 222 (2006).
- [13] D. C. Radford, Nucl. Instrum. Methods Phys. Res. A, **361**, 297 (1995).
- [14] K. S. Krane and R. M. Steffen, Phys. Rev. C **2**, 724 (1970).
- [15] R. M. Steffan and K. Alder, *The Electromagnetic Interaction in Nuclear Spectroscopy* (North-Holland, Amsterdam, 1975).
- [16] L. W. Fagg and S. S. Hanna, Rev. Mod. Phys. **31**, 711 (1959).
- [17] J. K. Deng, W. C. Ma, J. H. Hamilton, A. V. Ramayya, J. Rikovska, N. J. Stone, W. L. Croft, R. B. Piercey, J. C. Morgan, and P. F. Mantica, Jr., Nucl. Instrum. Methods Phys. Res. A, **317**, 242 (1992).
- [18] P. M. Jones, L. Wei, F. A. Beck, P. A. Butler, T. Byrski, G. Duchêne, G. de France, F. Hannachi, G. D. Jones, and B. Kharraja, Nucl. Instrum. Methods Phys. Res. A, **362**, 556 (1995).
- [19] K. Starosta *et al.*, Nucl. Instrum. Methods Phys. Res. A, **423**, 16 (1999).
- [20] T. Aoki, K. Furuno, Y. Tagishi, S. Ohya, and J. Ruan, At. Data. Nucl. Data. Tables **23**, 349 (1979).
- [21] E. Der Mateosian and A. W. Sunyar, At. Data. Nucl. Data. Tables **13**, 391 (1974).
- [22] R. Palit, H. C. Jain, P. K. Joshi, S. Nagaraj, B. V. T. Rao, S. N. Chintalapudi, and S. S. Ghugre, Pramana **54**, 347 (2000).
- [23] T. Yamazaki, Nucl. Data. A **3**, 1 (1967).
- [24] P. Mason *et al.*, Phys. Rev. C **71**, 014316 (2005).
- [25] K. S. Krane and R. M. Steffan, Phys. Rev. C **2**, 724 (1970).
- [26] *NNDC Online Data Service*, <http://www.nndc.bnl.gov>.
- [27] F. Ajzenberg-Selove, E. R. Flynn, S. Orbesen, and J. W. Sunier, Phys. Rev. C **15**, 1 (1977).
- [28] B. V. Pritychenko, T. Glasmacher, B. A. Brown, P. D. Cottle, R. W. Ibbotson, K. W. Kemper, and H. Scheit, Phys. Rev. C **66**, 051601(R) (2000).
- [29] S. J. Skorka, J. Hertel, and T. W. Retz-Schmidt, Nucl. Data. A **2**, 347 (1966).
- [30] M. R. Nixon, G. D. Jones, P. R. G. Lornie, A. Nagel, P. J. Nolan, H. G. Price, and P. J. Twin,

- J. Phys. G: Nucl. Phys. **1**, 430 (1975).
- [31] W. A. Sterrenburg, G. Van Middlekoop, and F. E. H. Van Eijkern, Nucl. Phys. A **275**, 48 (1997).
- [32] B. A. Brown and W. D. M. Rae, *MSU-NSCL Report* (2007).
- [33] E. K. Warburton, J. A. Becker, and B. A. Brown, Phys. Rev. C **41**, 1147 (1990).
- [34] B. A. Brown, <http://www.nsl.mscl.msu.edu/~brown/resources/SDE.HTM#a34t2>.
- [35] M. Ionescu-Bujor *et al.*, Phys. Rev. C **73**, 024310 (2006).
- [36] P. Wagner, J. P. Coffin, M. A. Ali, D. E. Alburger, and A. Gallmann, Phys. Rev. C **7**, 2418 (1973).
- [37] C. E. Ragan, C. E. Moss, R. V. Poore, N. R. Roberson, G. E. Mitchell, and D. R. Tilley, Phys. Rev. **188**, 1806 (1969).

TABLE I: Comparison of theoretical and experimental asymmetry and theoretical and experimental R_{DCO} values in ^{33}P and $^{33,34}\text{S}$

E_γ [keV]	Mixing ratio (δ)from NNDC	Δ_{IPDCO} (Experimental)	Δ_{IPDCO} (Theoretical)	R_{DCO} (Experimental)	R_{DCO} (Theoretical)
^{34}S					
2127	0.0	0.053(24)	0.043		1.00
2561	0.0	0.032(22)	0.019	0.99(6)	1.00
1001	-0.05	0.032(19)	0.051	0.57(3)	0.49
1066	0.0	0.068(25)	0.067	1.20(7)	1.20
^{33}P					
1848	-0.03	0.050(20)	0.045	1.76(34)	
1432	-0.60	-0.022(20)	-0.002	0.89(6)	
416	0.09	-0.188(29)	-0.135	0.87(6)	
2379	0.01	0.017(15)	-0.014	0.48(10)	0.49
1413	0.0	0.048(10)	0.046	0.94(6)	1.01
^{33}S					
968	-0.02	0.032(11)	0.047	0.84(6)	
1968	-0.56	0.005(9)	0.004	1.51(18)	1.67

TABLE II: The transition energies, excitation energies, relative intensities, initial and final spin-parities, multipolarities and the γ -ray branching ratios in $^{33,34}\text{P}$ and ^{33}S .

$E_\gamma^{[1]}$ [keV]	E_x [keV]	I_γ (%)	J_i^π	J_f^π	Multipolarity	Branching ratios (%)	
						Present work	Previous work
^{33}P							
186.2	5640	33.2(12)	11/2 ⁻	9/2 ⁻	(M1)	41.0(18)	46±2 ^b
237.0	4227	<i>weak</i>	7/2 ⁻				
247.0	5454	<i>weak</i>	9/2 ⁻				
416.4	1848	6.95(22)	5/2 ₁ ⁺	3/2 ⁺	M1+E2	6.50(28)	7±4 ^a
736.2	4227	8.25(27)	7/2 ⁻	5/2 ⁺	(E1)	7.76(34)	11±2 ^b
979.5	5207	<i>weak</i>		7/2 ⁻			
993.7	5221	<i>weak</i>		7/2 ⁻	(D)		
1008.0	5235	<i>weak</i>		7/2 ⁻			
1028.3	7966	2.18(8)	17/2 ⁽⁺⁾	15/2 ⁽⁻⁾	(E1)		
1226.8	5454	50.2(16)	9/2 ⁻	7/2 ⁻	(M1)	91.5(40)	100 ^b
1298.1	6938	5.45(19)	15/2 ⁽⁻⁾	11/2 ⁻	(E2)		
1311.5	6952	<i>weak</i>		11/2 ⁻	(D)		
1412.6	5640	47.8(16)	11/2 ⁻	7/2 ⁻	E2+M3	59.0(24)	54±2 ^b
1432.1	1432	> 18.95	3/2 ⁺	1/2 ⁺	M1+E2	100	100 ^a
1642.7	3491	6.93(25)	5/2 ₂ ⁺	5/2 ₁ ⁺	Q	54.1(24)	62±2 ^a
1780.5	3629	3.86(15)	7/2 ⁺	5/2 ₁ ⁺	(M1)	36.9(17)	28±3 ^a
1825.1	5454	4.68(15)	9/2 ⁻	7/2 ⁺	D	8.5(37)	
1848.1	1848	100(3)	5/2 ₁ ⁺	1/2 ⁺	E2+M3	93.5(39)	93±4 ^a
2058.8	3491	5.25(19)	5/2 ₂ ⁺	3/2 ⁺	(M1)	41.0(18)	38±4 ^a
2141.6	3990	1.45(7)		5/2 ₁ ⁺	(Q)		
2196.5	3629	6.60(21)	7/2 ⁺	3/2 ⁺	(E2)	63.1(25)	72±3 ^a
2378.8	4227	98.0(30)	7/2 ⁻	5/2 ₁ ⁺	E1+M2	92.2(39)	89±2 ^a

continued...

TABLE II: continued...

$E_\gamma^{[1]}$ [keV]	E_x [keV]	I_γ (%)	J_i^π	J_f^π	Multipolarity	Branching ratios (%)	
						Present work	Previous work
3606.0	5454	<i>weak</i>	9/2 ⁻	5/2 ₁ ⁺	(M2)		
3491.1	3491	0.62(3)	5/2 ₂ ⁺	1/2 ⁺	(E2)	4.84(26)	< 4 ^a
<hr/> ³⁴ P <hr/>							
429.4	429	100(3)	2 ⁺	1 ⁺	M1+E2	100	
679.4	4630	3.17(16)	6 ⁽⁻⁾	5 ⁽⁻⁾	(M1)	42.9(31)	
1047.8	3353	17.10(91)	5 ⁽⁻⁾	4 ⁽⁻⁾	(M1)		
1179.8	1609	0.74(10)	1 ⁽⁺⁾	2 ⁺	(M1)		
1443.7	3749	<i>weak</i>		4 ⁽⁻⁾			
1607.1	6237	4.50(45)	7 ⁽⁺⁾	6 ⁽⁻⁾	(E1)	40.5(41)	
1646.2	3951	3.60(43)	5 ⁽⁻⁾	4 ⁽⁻⁾	(M1)		
1637.7	3943	<i>weak</i>		4 ⁽⁻⁾			
1876.1	2305	88.6(11)	4 ⁽⁻⁾	2 ⁺	(M2+E3)	100	
1891.6	2321	11.28(88)	(3 ⁻)	2 ⁺	(E1+M2)		
2325.1	4630	4.22(30)	6 ⁽⁻⁾	4 ⁽⁻⁾	(E2)	57.1(48)	
2884.3	6237	6.61(40)	7 ⁽⁺⁾	5 ⁽⁻⁾	(M2)	59.5(48)	
3931.7	6237	<i>weak</i>	7 ⁽⁺⁾	4 ⁽⁻⁾			
<hr/> ³³ S <hr/>							
597.0	5990						
597.0	5393			(11/2 ⁻)			
602.5	3539	0.11(1)		7/2 ⁻			
841.1	841	> 0.63	1/2 ⁺	3/2 ⁺	(M1+E2)		
845.1	3781	0.67(3)	(9/2 ⁺)	7/2 ⁻	(E1)		
968.4	2936	48.5(17)	7/2 ⁻	5/2 ⁺	E1+M2	51.0(23)	50 ^c
1015.3	4796	0.37(2)	(11/2 ⁻)	(9/2 ⁺)	(E1)		
1126.5	1968	0.63(2)	5/2 ⁺	1/2 ⁺	(E2)	0.63(3)	< 1.5 ^c

continued...

TABLE II: continued...

$E_\gamma^{[1]}$ [keV]	E_x [keV]	I_γ (%)	J_i^π	J_f^π	Multipolarity	Branching ratios (%)	
						Present work	Previous work
1931.2	4867	0.62(3)		7/2 ⁻			
1967.6	1968	100(3)	5/2 ⁺	3/2 ⁺	M1+E2	99.4(42)	100 ^c
2935.6	2936	46.7(16)	7/2 ⁻	3/2 ⁺	(M2+E3)	49.0(27)	50 ^c

[1] The quoted energies are within ± 1 keV.

[2] ^aRef. [36]

[3] ^bRef. [30]

[4] ^cRef. [37]

TABLE III: Reduced transition probabilities for 1876 keV transition in ^{34}P considering both M2/E3 mixing and E2/M3 mixing. The lifetime range has been taken from the reported values of Asai *et al.* [2]. The mixing ratios are from our polarization measurements.

Half-life (ns)	Mixing ratio (δ)	Reduced transition probabilities			
		M2/E3		E2/M3	
		$B(M2)$ (<i>W.u.</i>)	$B(E3)$ (<i>W.u.</i>)	$B(E2)$ (<i>W.u.</i>)	$B(M3)$ (<i>W.u.</i>)
0.3	-1.03	0.207	372.681	0.006	12520.654
	-0.27	0.397	49.191	0.012	1652.638
2.5	-1.03	0.025	44.722	0.001	1502.478
	-0.27	0.048	5.903	0.001	198.317

TABLE IV: Comparison between experimental and theoretical transition energies, excitation energies, mixing ratios and reduced transition probabilities in ^{35}S and ^{37}Ar .

$E_\gamma[\text{keV}]$		$E_x(J^\pi)[\text{keV}]$		$\tau[\text{ns}]$	δ		$B(M2)$ [W.u.]		$B(E3)$ [W.u.]	
Expt.	Theo.	Expt.	Theo.	from NNDC	Expt.	Theo.	Expt.	Theo.	Expt.	Theo.
^{35}S										
1911	2738	1911	2738	1.02(5)	-0.19(8)	-0.05	0.088(5)	0.196	4.62	0.38
^{37}Ar										
1611	2680	1611	2680	4.37(9)	-0.12(1)	-0.08	0.058(13)	0.112	1.7(3)	0.50

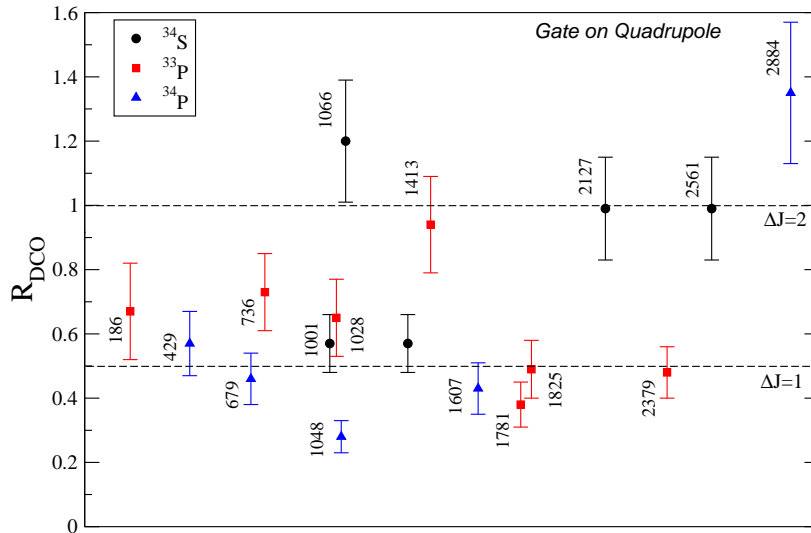


FIG. 1: “(Color online)” The experimental R_{DCO} values for transitions in $^{33,34}\text{P}$ and $^{33,34}\text{S}$ when the gate is on a quadrupole transition.

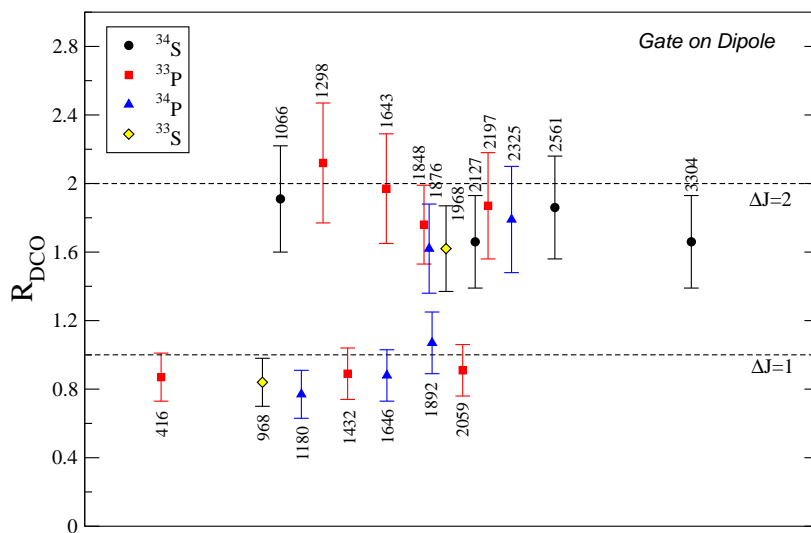


FIG. 2: “(Color online)” The experimental R_{DCO} values for transitions in $^{33,34}\text{P}$ and $^{33,34}\text{S}$ when the gate is on a quadrupole transition.

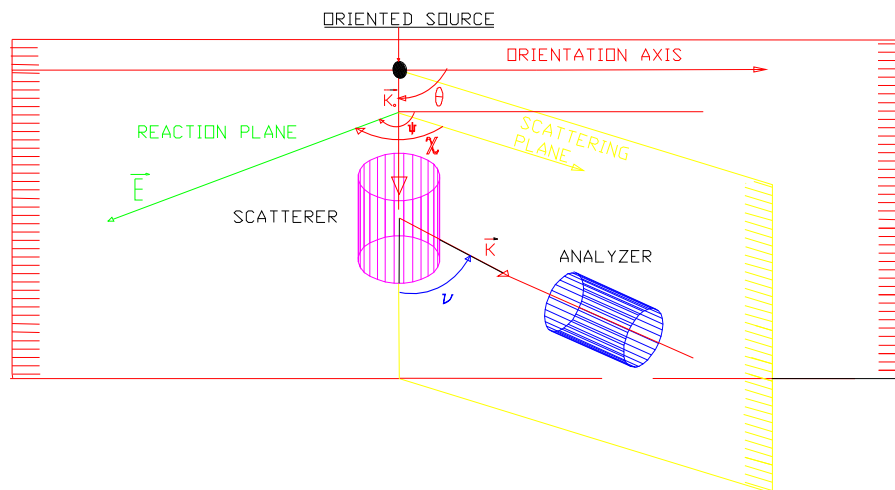


FIG. 3: “(Color online)” Schematic diagram of the geometry of a Compton polarimeter

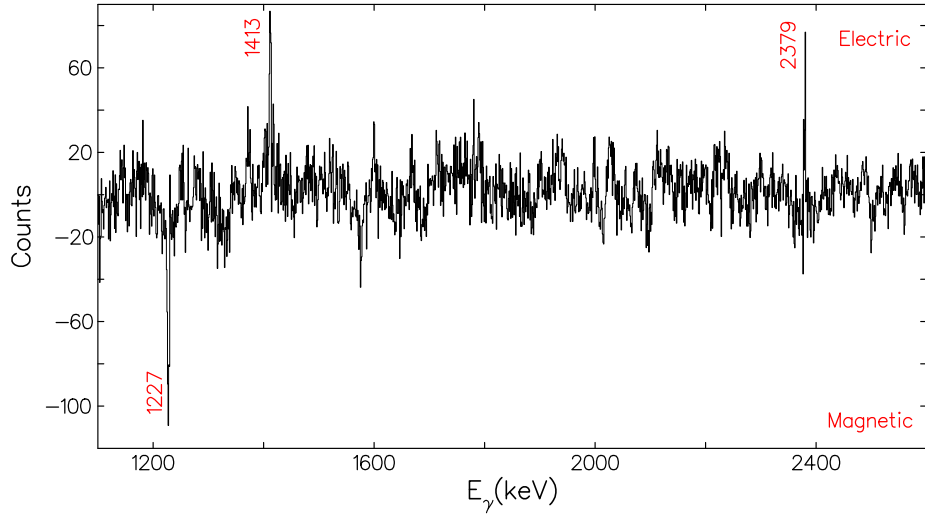


FIG. 4: “(Color online)” Background subtracted difference spectrum for perpendicular and parallel coincidences. The positive peaks indicate electric transitions and the negative peaks indicate magnetic transition. Gate is on 1848 keV ($5/2^+ \rightarrow 1/2^+$) in ^{33}P .

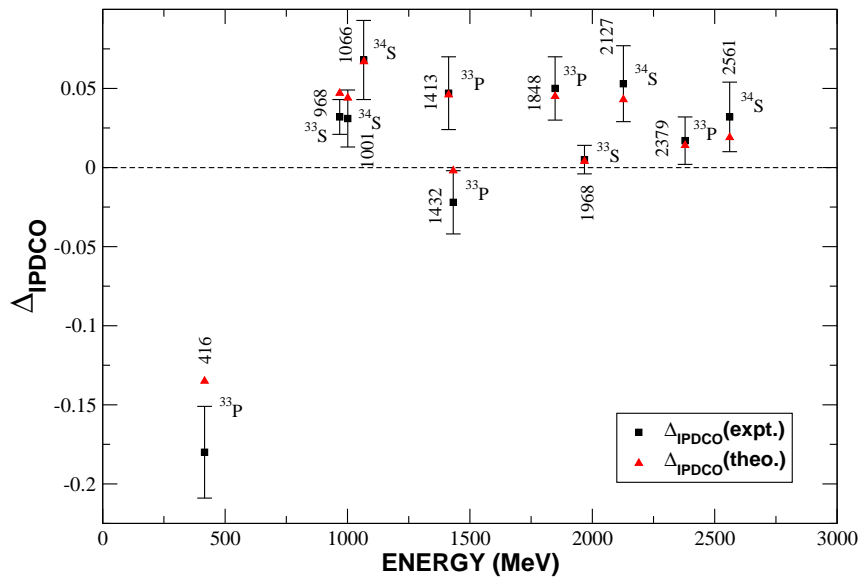


FIG. 5: “(Color online)” Theoretical and experimental Δ_{IPDCO} as a function of gamma ray energy.

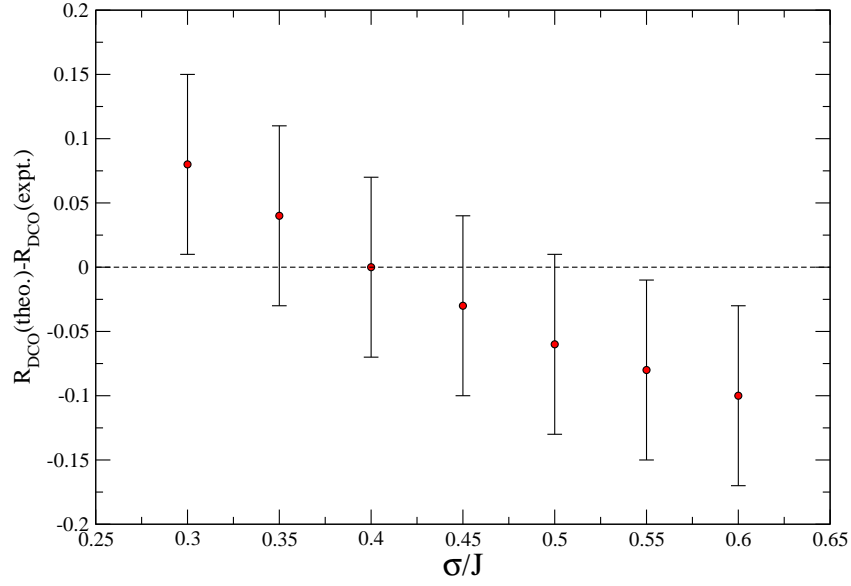


FIG. 6: “(Color online)” Plot of the difference between theoretical and experimental R_{DCO} as a function of σ/J for 1066 keV transition ($5^- \rightarrow 3^-$) in ^{34}S .

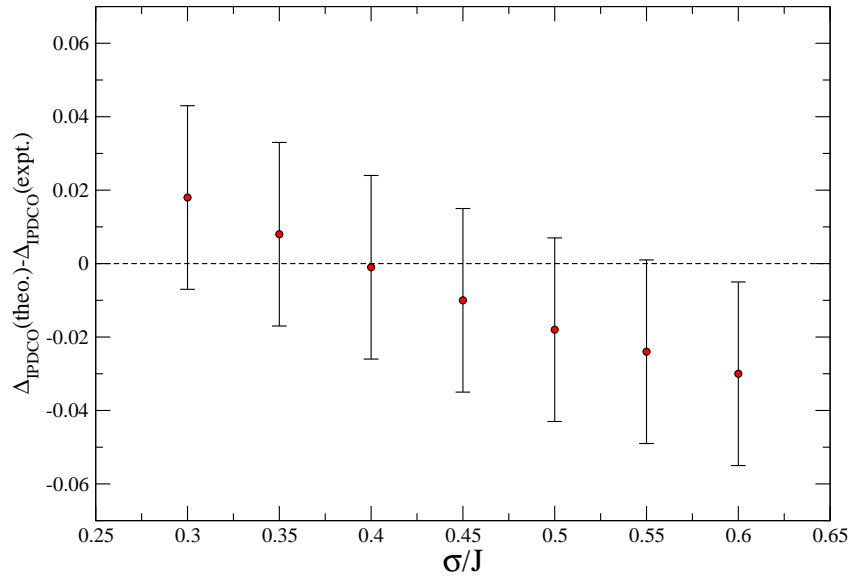


FIG. 7: “(Color online)” Plot of the difference between theoretical and experimental Δ_{IPDCO} as a function of σ/J for 1066 keV transition ($5^- \rightarrow 3^-$) in ^{34}S .

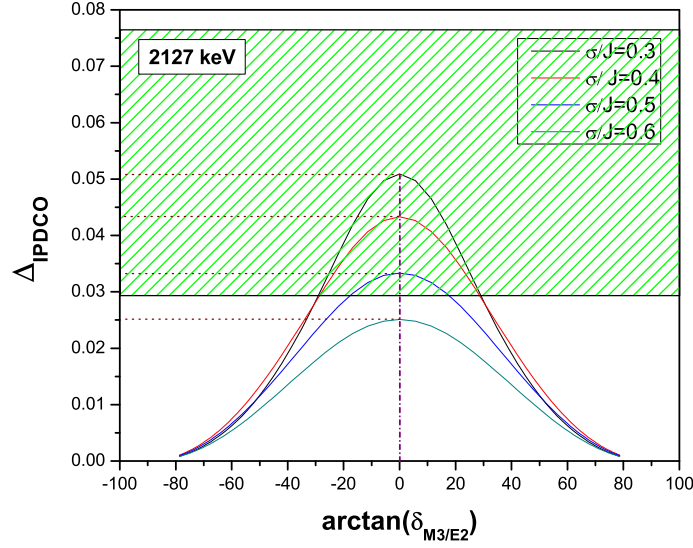


FIG. 8: “(Color online)” Plot of theoretical Δ_{IPDCO} as a function of mixing ratios at different σ/J for 2127 keV ($2^+ \rightarrow 0^+$) in ^{34}S . The shaded area represents the range of experimentally measured Δ_{IPDCO} . The shell model predicted mixing ratio and the corresponding Δ_{IPDCO} values at different σ/J are marked by the vertical and the horizontal dotted lines respectively.

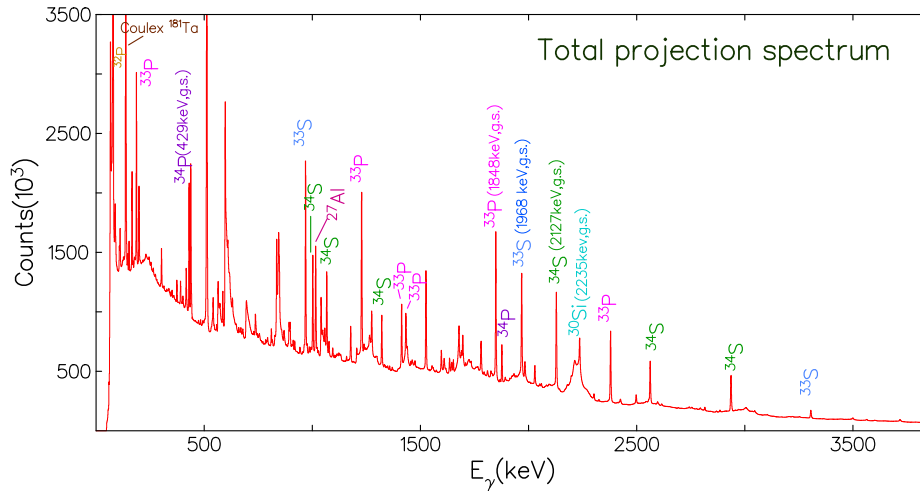


FIG. 9: Projection spectrum from $^{18}\text{O}+^{18}\text{O}$ fusion reaction at an incident beam energy of 34 MeV.

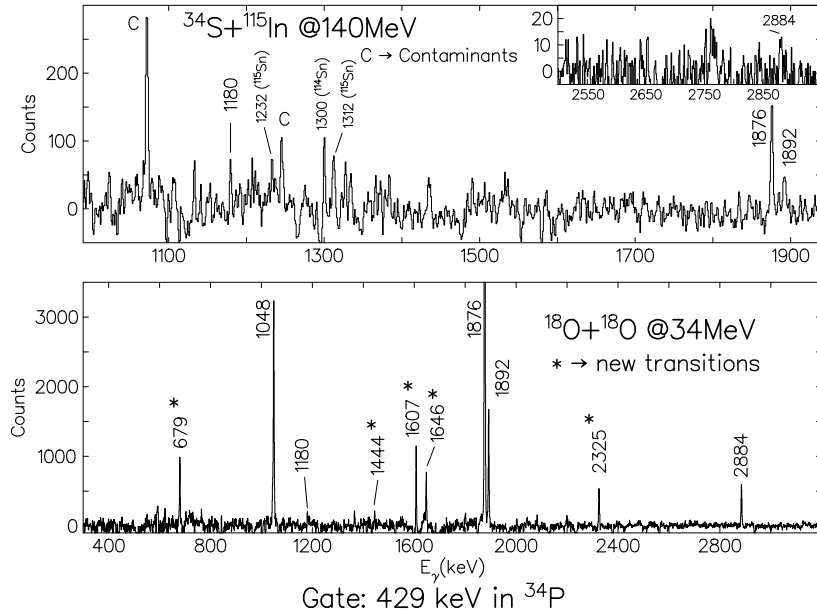


FIG. 10: Coincidence spectrum with gate set on 429 keV in ^{34}P from: transfer/deep-inelastic reaction [5] (top panel) and present reaction (bottom panel). This figure highlights the advantage of the fusion reaction over non-equilibrated reactions to populate nuclei in and around the "island of inversion".

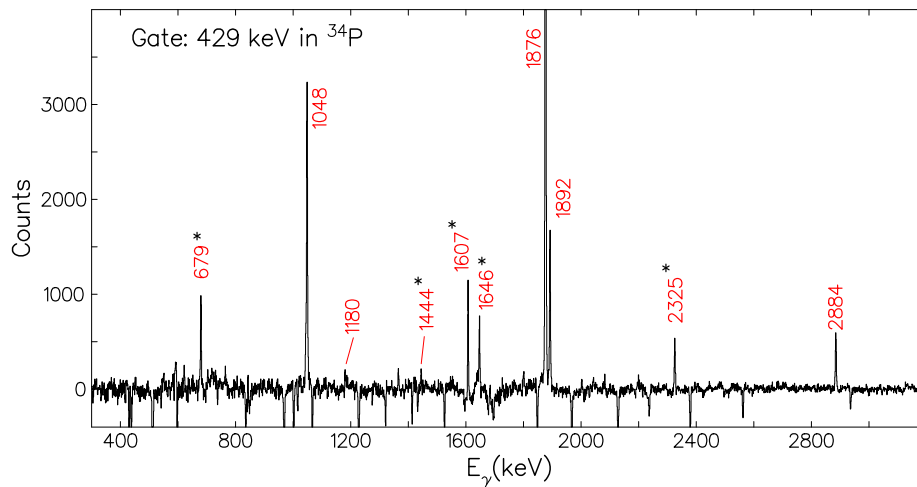


FIG. 11: "(Color online)" Coincidence spectrum with gate on 429 keV in ^{34}P . The new assigned γ -rays are marked with an asterisk.

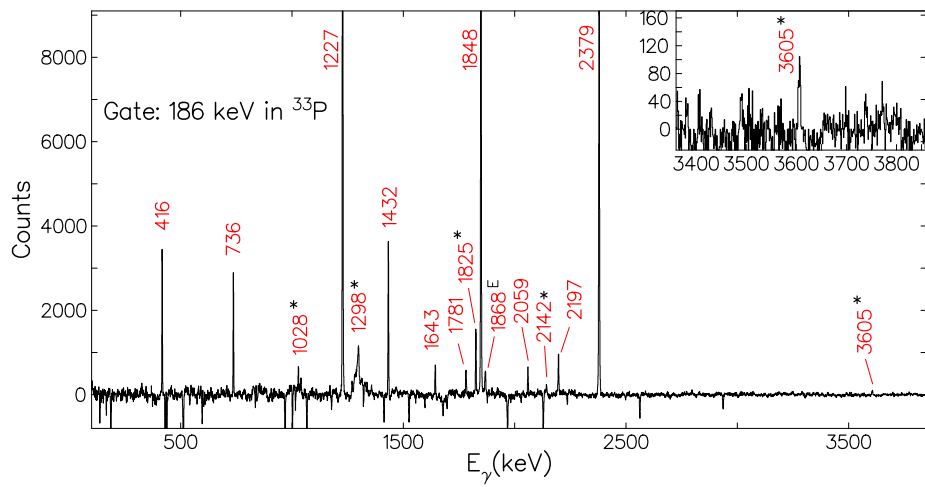


FIG. 12: “(Color online)” Coincidence spectrum with gate on 186 keV in ^{33}P . The new assigned γ -rays are marked with an asterisk.

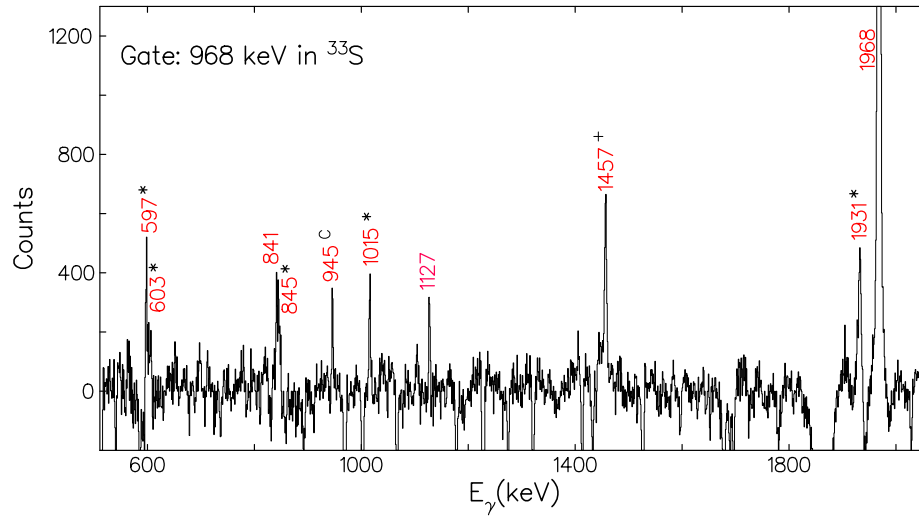


FIG. 13: “(Color online)” Coincidence spectrum with gate on 968 keV in ^{33}S . The new assigned γ -rays are marked with an asterisk. 945-keV is a contaminant (C) from ^{30}Si . 1457-keV(+) was found to be in coincidence with the 968- and the 841-keV transitions, but could not be placed in the level scheme of ^{33}S from coincidence arguments.

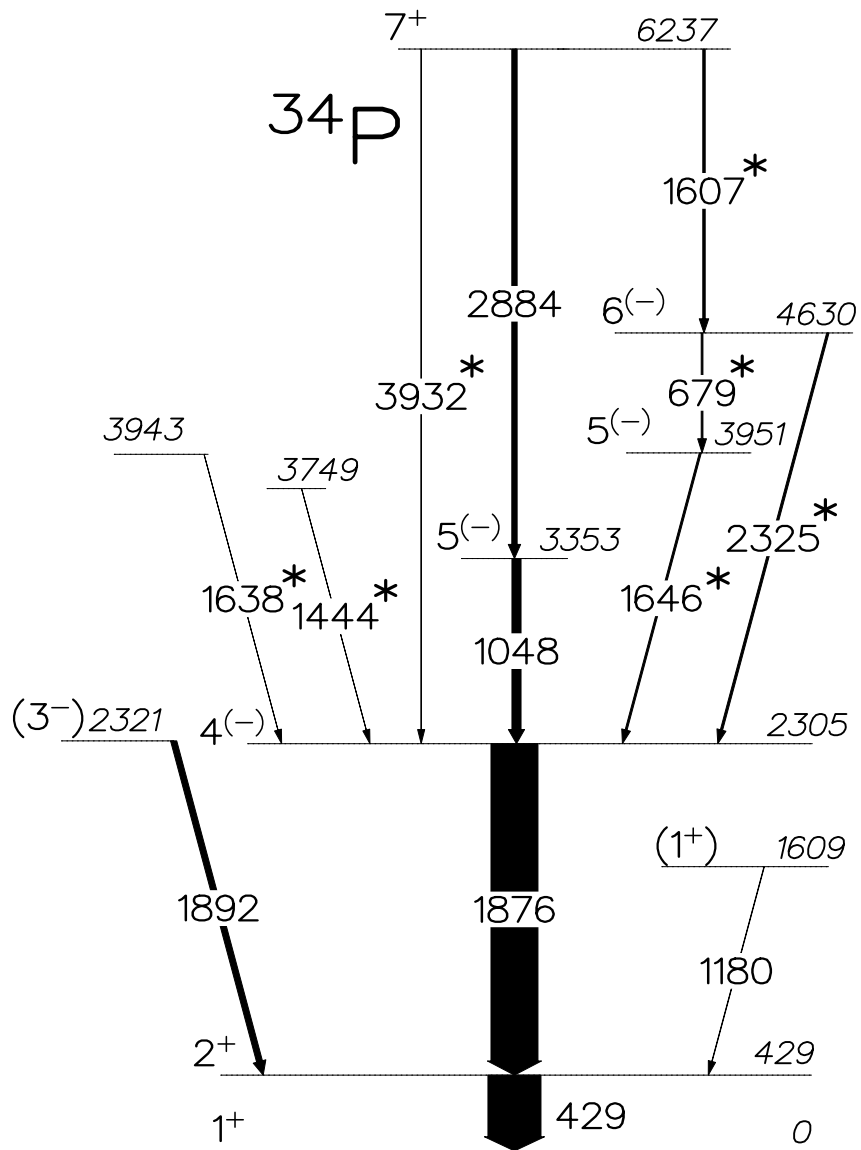


FIG. 14: Level scheme of ^{34}P . The new transitions are indicated by an asterisk. The width of the arrows connecting the levels is proportional to the relative γ -ray intensities.

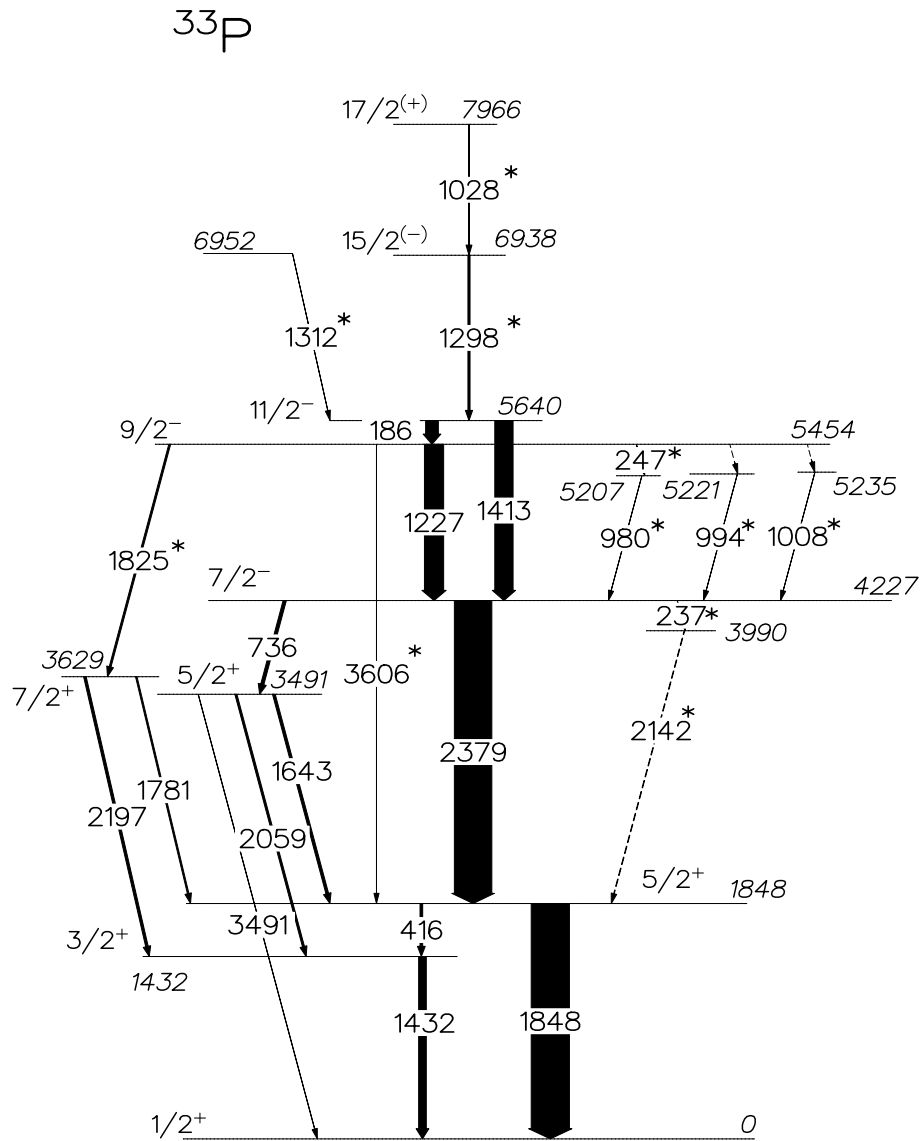


FIG. 15: Level scheme of ^{33}P . The new transitions are indicated by an asterisk. The width of the arrows connecting the levels is proportional to the relative γ -ray intensities.

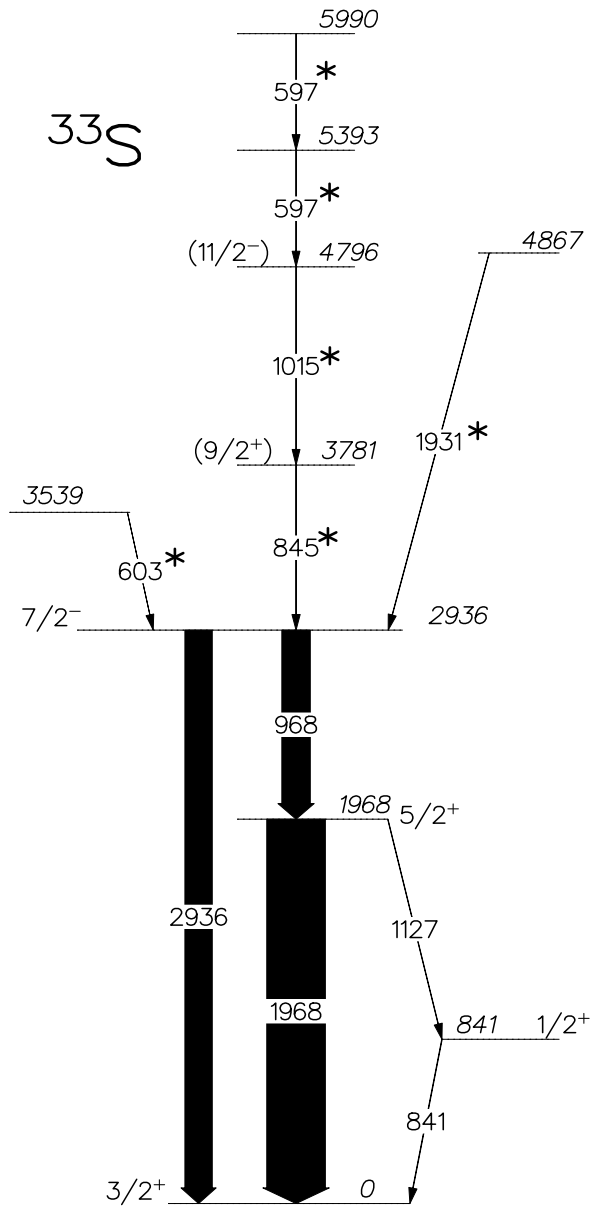


FIG. 16: Level scheme of ^{33}S . The new transitions are indicated by an asterisk. The width of the arrows connecting the levels is proportional to the relative γ -ray intensities.

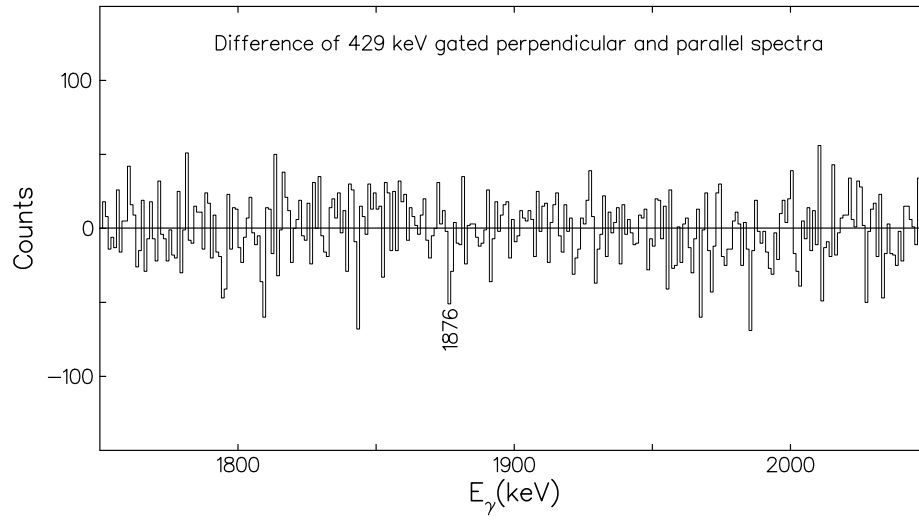


FIG. 17: Background subtracted difference spectrum of perpendicular and parallel scattered events when gated by 429 keV transition in ^{34}P . Absence of a clear positive or negative peak at 1876 keV is indicative of its mixed nature.

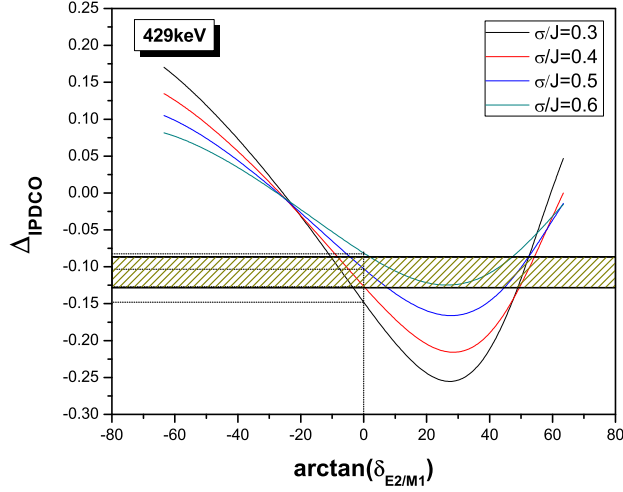


FIG. 18: “(Color online)” Plot of theoretical Δ_{IPDCO} as a function of mixing ratios at different σ/J for 429 keV ($2^+ \rightarrow 1^+$) in ^{34}P . The shaded area represents the range of experimentally measured Δ_{IPDCO} . The shell model predicted mixing ratio and the corresponding Δ_{IPDCO} values are marked by the vertical and the horizontal dotted lines respectively.

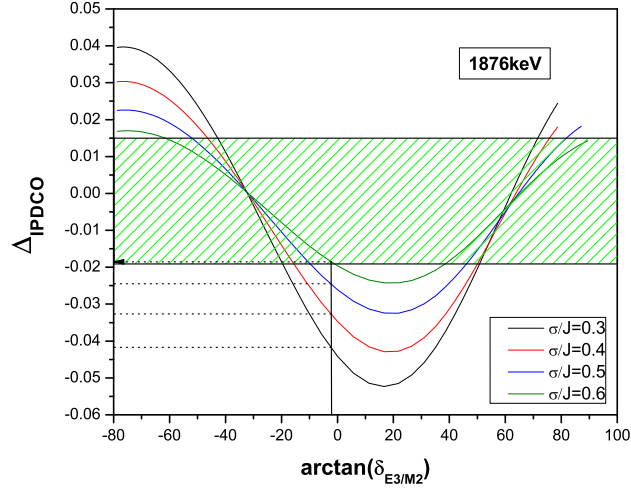


FIG. 19: “(Color online)” Plot of theoretical Δ_{IPDCO} as a function of mixing ratios at different σ/J for 1876 keV ($4^- \rightarrow 2^+$) in ^{34}P considering a M2+E3 distribution. The shaded area represents the range of experimentally measured Δ_{IPDCO} . The shell model predicted mixing ratio and the corresponding Δ_{IPDCO} values are marked by the vertical and the horizontal dotted lines respectively.

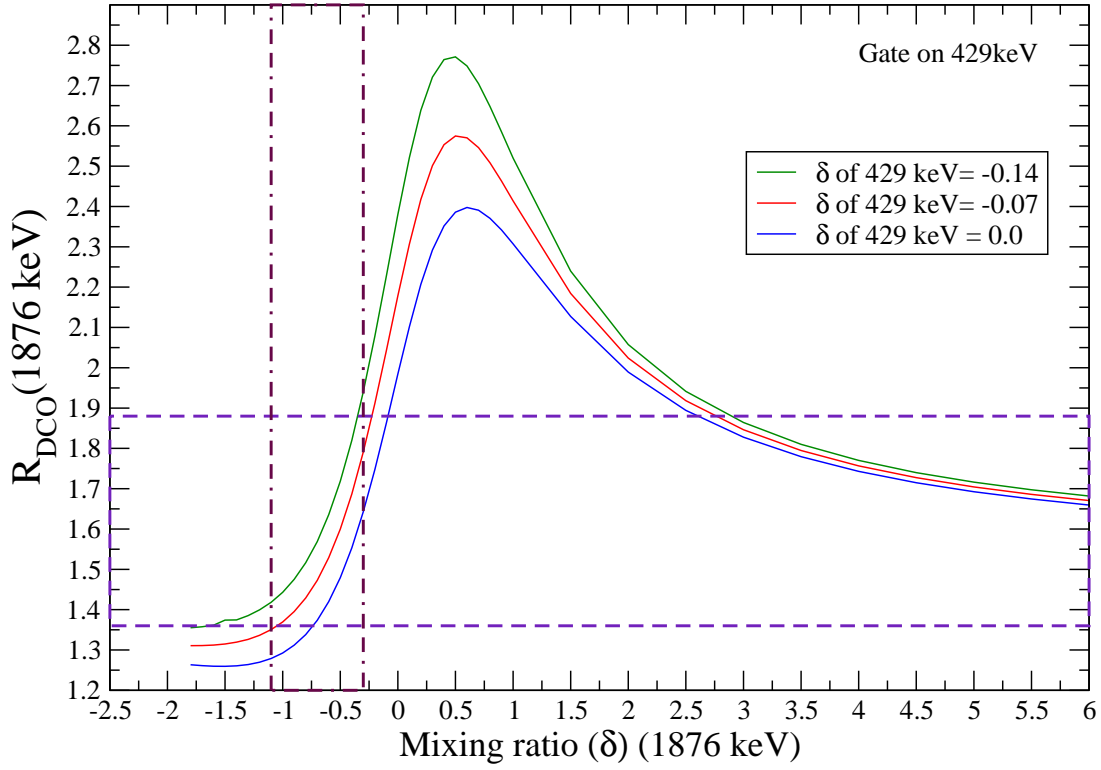
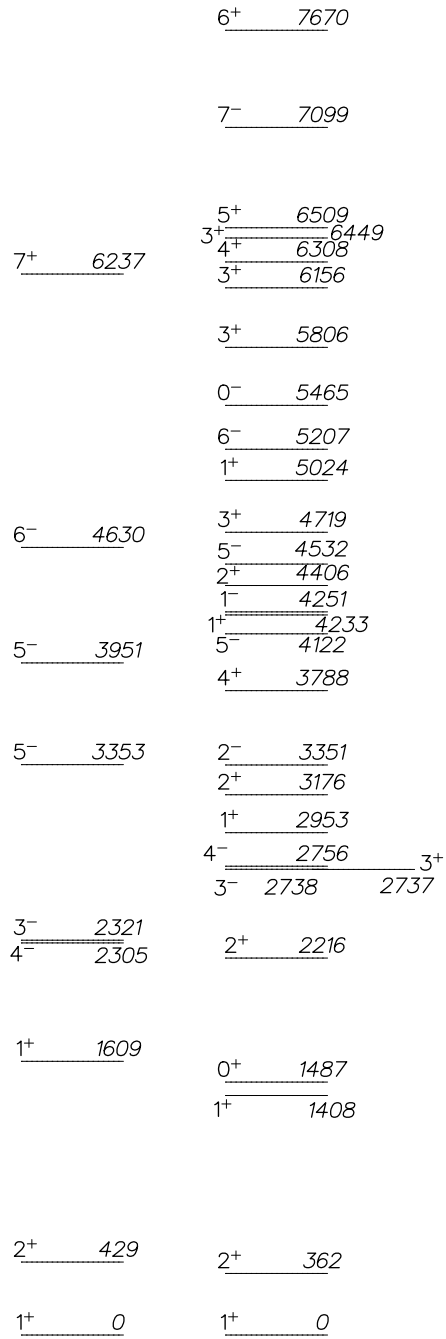


FIG. 20: “(Color online)” The variation in R_{DCO} for 1876 keV as a function of its mixing ratio at 3 different values of mixing ratio of 429 keV (the gating transition).



Experimental

Shell Model

FIG. 21: Comparison between experimental and shell model predicted levels in ^{34}P .